Published in final edited form as:
J Immunol. 2007 May 1; 178(9): 5496–5504.

Krüppel-Like Transcription Factor 13 Regulates T Lymphocyte Survival In Vivo[1]

Meixia Zhou[*], **Lisa McPherson**[*], **Dongdong Feng**[*], **An Song**[†], **Chen Dong**[*], **Shu-Chen Lyu**[*], **Lu Zhou**[*], **Xiaoyan Shi**[*], **Yong-Tae Ahn**[*], **Demin Wang**[‡], **Carol Clayberger**[*], and **Alan M. Krensky**[*,2]

[*]*Department of Pediatrics, Stanford University, Palo Alto, CA 94305*

[†]*Genentech, South San Francisco, CA 94080*

[‡]*Blood Research Institute, Blood Center of Wisconsin and Department of Microbiology and Molecular Genetics, Medical College of Wisconsin, Milwaukee, WI 53226*

Abstract

Krüppel-like transcription factor (KLF)13, previously shown to regulate RANTES expression in vitro, is a member of the Krüppel-like family of transcription factors that controls many growth and developmental processes. To ascertain the function of KLF13 in vivo, *Klf13*-deficient mice were generated by gene targeting. As expected, activated T lymphocytes from *Klf13*$^{-/-}$ mice show decreased RANTES expression. However, these mice also exhibit enlarged thymi and spleens. TUNEL, as well as spontaneous and activation-induced death assays, demonstrated that prolonged survival of *Klf13*$^{-/-}$ thymocytes was due to decreased apoptosis. Microarray analysis suggests that protection from apoptosis-inducing stimuli in *Klf13*$^{-/-}$ thymocytes is due in part to increased expression of BCL-X_L, a potent antiapoptotic factor. This finding was confirmed in splenocytes and total thymocytes by real-time quantitative PCR and Western blot as well as in $CD4^+CD8^-$ single-positive thymocytes by real-time quantitative PCR. Furthermore, EMSA and luciferase reporter assays demonstrated that KLF13 binds to multiple sites within the *Bcl-X_L* promoter and results in decreased *Bcl-X_L* promoter activity, making KLF13 a negative regulator of BCL-X_L.

Exposure of T cells to foreign Ag generates activated effector cells through a process involving activation, proliferation, differentiation, and, finally, lymphocyte death. Changes in gene expression, central to each of these steps, are controlled by transcription factors that specifically bind to promoter elements and act as positive or negative regulators of transcription. Krüppel-like transcription factors (KLFs)[3] regulate a large number of genes controlling growth and development that have GC-rich promoters (1). To date, 17 distinct KLFs have been identified, and all contain a highly conserved DNA-binding domain at the C terminus composed of three tandem Cys_2His_2 zinc-finger motifs, a variable amino terminus that contains activation or repression domains, and nuclear localization sequences adjacent to or within the zinc-finger domain.

[1]This work was supported by a grant from the National Institutes of Health (DK35008). A.M.K. is the Shelagh Galligan Professor of Pediatrics.

2Address correspondence and reprint requests to Dr. Alan M. Krensky, Department of Pediatrics, Stanford University, 300 Pasteur Drive, Stanford, CA 94305. E-mail address: krensky@stanford.edu .

Disclosures

The authors have no financial conflict of interest.

[3]Abbreviations used in this paper: KLF, Krüppel-like transcription factor; RFLAT, RANTES factors of late-activated T lymphocyte; ES, embryonic stem; RT, room temperature; rt-qPCR, real-time quantitative PCR; Ct, cycle threshold; SP, single positive.

We identified KLF13 as the dominant transcription factor controlling expression of the chemokine RANTES in T lymphocytes (2). RANTES, which has been implicated in a myriad of human diseases as diverse as AIDS, cancer, heart disease, asthma, diabetes, and organ transplant rejection, is expressed within hours in activated fibroblasts and epithelial cells, depending only upon Rel proteins for expression (3–5). In contrast, regulation of late expression of RANTES in T lymphocytes is complex (6). Expression cloning identified a number of regulatory proteins controlling RANTES expression in T lymphocytes (2,7), including p50 and p65 Rel proteins as well as novel factors, designated RANTES factors of late-activated T lymphocytes (RFLAT)-1 (KLF13) (2,8) and RFLAT-2 (stromelysin-1 platelet-derived growth factor-responsive element binding protein) (9). In T lymphocytes, KLF13 is translationally regulated, providing a rheostat mechanism for rapid expression of RANTES in effector and memory T cells (10). In addition, KLF13 activates the promoters for SV40, γ-globin, and SM22α and represses the promoter for cytochrome P450 CYP1A1 in vitro, indicating that the regulatory activity of KLF13 is in part tissue and/or promoter dependent (11–14).

To more fully understand the in vivo role of KLF13, mice lacking the *Klf13* gene were generated by gene targeting. As predicted from the in vitro studies, expression of RANTES is decreased in activated T lymphocytes from $Klf13^{-/-}$ mice. However, these mice also exhibit increased numbers of lymphoid cells, suggesting that KLF13 regulates genes involved in lymphocyte proliferation and/or death. Although no differences in proliferation were observed in bone marrow or thymocytes from $Klf13^{-/-}$ when compared with $Klf13^{-/-}$ mice, both thymocytes and splenocytes of $Klf13^{-/-}$ mice were more resistant to apoptotic stimuli. Expression of BCL-X_L, a potent antiapoptotic factor, is elevated in thymocytes and splenocytes from $Klf13^{-/-}$ mice, and in reporter gene assays, KLF13 suppresses transcription driven by the *Bcl-xL* promoter. Thus, KLF13 is a positive regulator of RANTES and a negative regulator of BCL-X_L in thymocytes and splenocytes.

Materials and Methods

Gene targeting

The knockout plasmid was constructed using the pKO Scrambler NTKV-1901 vector as a backbone (Stratagene). A 5.1-kb genomic fragment immediately downstream of *Klf13* exon 1 and a 1.9-kb fragment upstream of exon 1 were subcloned either 5′ or 3′ of the *Neo* gene on the vector to generate a targeting vector (Fig. 1*A*). This targeting vector was linearized with *Not*I restriction digestion and electroporated into embryonic stem (ES) cells (129Sv) by the Stanford Transgenic Facility. Neomycin-resistant ES cell clones were screened for homologous recombination by PCR. Primers for amplifying the *Klf13* allele were 5′-CTCGGTAATGTCCCGCCCATA-3′ and 5′-AGAGTCGGCCTGTCTTAGGGA-3′; primers for amplifying the replaced *Neo* gene were 5′-CTCGGTAATGTCCCGCCCATA-3′ and 5′-AAGCCGGTCTTGTCAATCAGGATGATCTGGACG-3′. Recombinant ES cells were confirmed by Southern blot analysis of *Bam*HI-digested genomic DNA hybridized to a 0.9-kb probe (Fig. 1*A*).

Mice

Two *Klf13*-targeted clones were injected into C57BL/6J blastocysts. Chimeras from these clones were mated with C57BL/6J females (The Jackson Laboratory). Germline transmission of the targeted *Klf13* allele was detected and heterozygous mice were backcrossed with C57BL/6J mice for six generations. Mice heterozygous for the mutant gene were then interbred to homozygosity. All mice were analyzed at the age of 11–12 wk, unless otherwise indicated. All studies performed in mice were reviewed and approved by the Stanford University Institutional Review Board.

Western blot

Whole cell extracts from thymi and spleens were prepared using Nonidet P-40 lysis buffer (250 mM NaCl, 1% Nonidet P-40, 0.25 M sodium deoxycholate, 50 mM Tris buffer (pH 8), 2 mM EDTA, 1 mM PMSF, 10 μg/ml leupeptin, and 10 μg/ml aprotinin). Total protein (20 μg) was resolved by 10% SDS-PAGE and transferred to polyvinylidene difluoride membrane. Western blot was performed using Abs specific for BCL-X_L (BD Biosciences), KLF13 (2), TUBA1 (Abcam), or JAB1 (Santa Cruz Biotechnology). Protein bands were detected by ECL (Amersham Biosciences).

T lymphocyte isolation and RANTES ELISA

T lymphocytes were isolated by magnetic bead depletion of non-T lymphocytes using a MACS Pan T Cell Isolation kit (Miltenyi Biotec). For ELISA, monoclonal anti-mouse RANTES Ab (2 μg/ml, 100 μl/well, 96-well microtiter plates; R&D Systems) was used as the capture Ab and biotinylated goat anti-mouse RANTES polyclonal Ab (100 ng/ml, 100 μl/ well; R&D Systems) was used as the detecting Ab. Recombinant RANTES was purchased from R&D Systems. HRP-conjugated anti-goat Ab (1/1,000 dilution, 100 μl/well; BD Biosciences) was used to detect bound Ab. After washing, 3,3′, 5,5′-tetramethylbenzene was added and the plate was incubated at room temperature (RT) for 30 min. The reaction was stopped by addition of 50 μl of 2 N H_2SO_4 and absorbance was read at 450 nm.

Flow cytometric analysis and cell sorting

The following fluorescein (FITC)-, PE-, Cy-Chrome (PE-Cy5)-, or allophycocyanin-coupled Abs were obtained from BD Biosciences: CD3, CD4, CD8, CD45R/B220, NK1.1, and TCRβ. mAb specific for TCRγδ was purchased from Caltag Laboratories. Cells were blocked with unlabeled Abs against CD16 (FcRIII) and CD32 (FcRII) (Caltag Laboratories), stained on ice with optimal amounts of dye-coupled Abs diluted in staining medium (PBS, 2% BSA, 0.05% azide) for 30 min, then washed twice. Stained cells were analyzed by flow cytometry on a FACScan (BD Biosciences). Dead cells were excluded on the basis of scatter characteristics, and 10,000 events were acquired per sample. For cell sorting, total thymocytes were stained with Abs specific for mouse CD4 and CD8, and $CD4^+CD8^-$ cells were purified by cell sorting on a FACS Vantage (BD Biosciences).

BrdU uptake

In vivo labeling was performed using the FITC BrdU Flow Kit (BD Biosciences) according to the manufacturer's instructions. Briefly, mice were i.p. injected with 1 mg of BrdU and sacrificed 2 h later. Thymus and bone marrow cells were harvested, stained with FITC anti-BrdU and 7-aminoactinomycin D, and analyzed by flow cytometry on a FACScan (BD Biosciences).

CFSE labeling

Splenocytes, depleted of erythrocytes by hypotonic lysis, were suspended at a density of 2×10^7 cells/ml in PBS. An equal volume of 10 μM carboxy-fluorescein diacetate succinimidyl ester (CFDASE; Molecular Probes) in PBS was added and the cells were gently mixed for 10 min at 37°C. Unbound CFDASE, or the deacetylated form, CFSE, was quenched by the addition of an equal volume of FCS. FACS analysis of cells immediately following CFSE labeling indicated a labeling efficiency exceeding 99%. Labeled cells were cultured in vitro with anti-CD3 (0.2 μg/ml) and anti-CD28 (0.2 μg/ml) Abs (BD Biosciences). At the time of harvest (24, 48, 72, and 96 h), CFSE-labeled splenocytes were washed in cold PBS supplemented with 2% FCS and 0.01% sodium azide, and 10^6 cells per sample were stained with a combination of PE-conjugated CD4 and PECy5-conjugated CD8 Ab (BD Biosciences). TOPRO-3 (Molecular Probes) was used to distinguish live and dead cells. Four-color flow

cytometry was performed on a FACSCalibur dual-laser cytometer: 100,000 events were collected.

Apoptosis assays

TUNEL assay—An In Situ Cell Death Detection Kit (Roche Applied Science) was used to localize 3′ DNA strand breaks following the manufacturer's protocol. Briefly, 1.5×10^6 thymocytes were washed, permeabilized, fixed, then labeled at 37°C with TUNEL reaction mixture for 1 h. Labeled cells were analyzed by flow cytometry.

Spontaneous and activation-induced thymocyte death assays—Thymocytes were cultured in 48-well plates at 2×10^6 cells/ml in complete medium. Cells were incubated in medium with or without Con A (10 μg/ ml; Sigma-Aldrich). Cells were collected at 0, 3, 20, and 24 h followed by incubation with propidium iodide (4 μg/ml; Sigma-Aldrich) for 5 min at RT. Apoptosis was determined by flow cytometry, gating on the subdiploid population.

Staurosporine treatment

Freshly isolated cells (4×10^5 cells) were incubated at 37°C with 1 μM staurosporine in complete medium for 4 h and analyzed for annexin V and propidium iodide staining as described previously (15).

Microarray analysis

Total RNA was isolated using RNeasy Minikit (Qiagen) and genomic DNA was removed using the RNase-Free DNase Set (Qiagen). Methods for all procedures are detailed in protocols provided by the Stanford Functional Genomics Facility (http://www.microarray.org/sfgf/).

Real-time quantitative PCR (rt-qPCR)

cDNA was generated using the QuantiTect Reverse Transcription kit (Qiagen) from 1 μg of total RNA. rt-qPCR was performed in triplicate on 0.05 μg of cDNA using QuantiTect Primer Assays (Qiagen) and SYBR Green PCR Master Mix (Applied Biosystems). *GusB* expression was used as an endogenous control. rt-qPCR was performed on an ABI PRISM 7900-HT Sequence Detection System (Applied Biosystems). The expression of mRNA is represented as fold increase ($2^{-\Delta\Delta Ct}$), where $\Delta\Delta Ct = [\Delta Ct_{(-/-)}] - [\Delta Ct_{(+/+)}]$, and $\Delta Ct = [Ct_{(sample)}] - [Ct_{(Gusb)}]$.

EMSA

^{32}P-end-labeled probes corresponding to sequential 300-bp regions of the murine *Bcl-xL* promoter from −1800 to −1 bp relative to the translational start site were prepared using T4 PNK (New England Biolabs). These 300-bp regions were PCR amplified from mouse genomic DNA using the following primers designated by their position relative to the *Bcl-xL* translation start site: upstream primers (−1820 bp, 5′-ACGCGTCGCCTGAGACTCCTCAAATCGC-3′; −1499 bp, 5′-ACGCGTAGGTGAGAGCGCCGCCTC-3′; −1199 bp, 5′-ACGCGTCTCCAGAAGGCCGCCTTGG-3′; −897 bp, 5′-ACGCGTCTGTCTTCCCCCTGTCCGC-3′; −602 bp, 5′-AC GCGTGCAGGTTCCTAAGCTTCGCAATTCC-3′; −302 bp 5′-ACGCGTCGGATGAAACAATTCAAAGCTGGCTGG-3′) and downstream primers (−1500 bp, 5′-AGATCTGCGAGCCCCAGAGAGCCGT-3′; −1200 bp, 5′-AGATCTCCCCCTGCAGGGCTCGA-3′; −898 bp, 5′-AGATCT CCTCGGATCTGTGATCTGATTTCGG-3′; −600 bp, 5′-AGATCTTGCCCCCTCACAACCTGGTTC-3′; −300 bp, 5′-AGATCTCCTCCTCTTTTTACTACAACCACCC-3′; −1 bp, 5′-CTGAGATCTTTTTATAATAGAGATGGGCTCAACCAGTCC-3′). Recombinant GST-

tagged KLF13 expression plasmid (*Klf13*/pGEX4T-1) was constructed by sub-cloning full-length *Klf13* from RFLAT-1/pcDNA3.1(+) (2) into pGEX4T-1 (Amersham Biosciences). Recombinant GST derived from empty vector and GST-KLF13 was purified using glutathione Sepharose 4B according to the manufacturer's protocol. For EMSA, probe was incubated at RT for 30 min with 0.3 μg of purified GST derived from empty pGEX4T-1 vector or recombinant GST-tagged KLF13 in 20 mM HEPES (pH 7.9), 1 mM $MgCl_2$, 0.08 mM EGTA, 0.4 mM DTT, 40 mM KCl, 5% Ficoll, 1.25 mg/ml BSA, and 0.015 mg/ml poly(dI:dC) (Sigma-Aldrich). Supershift was performed by adding 1 μl of anti-KLF13 polyclonal rabbit antisera (2) or anti-p53 Ab (Santa Cruz Biotechnology). DNA-protein complexes were resolved on 4% nondenaturing acrylamide gels in 0.25× TBE buffer at 4°C. Gels were dried and exposed to film overnight.

Luciferase reporter assay

A series of luciferase reporter constructs comprised of nested deletions and sequential 300-bp regions of the murine *Bcl-xL* promoter were PCR-amplified and subcloned into the *Mlu*I and *Bgl*II sites of pGL3 basic (Promega). These were designated as −1,800/−1, −1,500/−1, −1,200/−1, −900/−1, −600/−1, −300/−1, −1,800/−1,500, −1,500/−1,200, −1,200/−900, −900/−600, and −600/−1 by the approximate region of upstream promoter relative to the translational start site present in each construct. The exact position and sequence of the primers used for PCR amplification of the deletion constructs were as described above for the EMSA probes. Murine KLF13 expression plasmid was constructed as described previously (2). NIH 3T3 cells (2.5×10^5) were transfected in triplicate using FuGENE 6 reagent (Roche Applied Science) and 2 μg of DNA comprised of 250 ng of specific *muBcl-xL*/pGL3 reporter construct and 1.75 μg of either murine KLF13 expression plasmid or pcDNA3.1(+) vector as a control. Cell extracts were harvested at 24 h and assayed for luciferase by luminometry using the luciferase reporter assay system (Promega). Luciferase activity was normalized by total cellular protein content assayed using a BCA protein quantitation kit (Pierce). Data ± SD are an average of three independent experiments.

Statistical analysis

ANOVA was used to determine differences of resistance to spontaneous and activation-induced cell death of thymocytes from $Klf13^{+/+}$ and $Klf13^{-/-}$ mice. Other variables were determined using unpaired Student's *t* test. Significance is considered at $p < 0.05$.

Results

Generation of *Klf13*-deficient mice

Homologous recombination in murine ES cells was used to produce a targeted mutation of the *Klf13* gene (Fig. 1*A*). The resultant null mutation deleted exon 1, encoding two-thirds of the entire *Klf13* gene, confirmed by PCR (data not shown) and Southern blotting (Fig. 1*B*). $Klf13^{+/-}$ ES cell clones were used to produce chimeric mice, which transmitted the targeted allele through the germline. Heterozygous mice were grossly normal and were backcrossed to the C57BL/6J strain for five generations to produce $Klf13^{-/-}$ mice on a pure genetic background.

In $Klf13^{+/+}$ mice, KLF13 is constitutively expressed in thymocytes (Fig. 1*C*, lanes 1 and 3). In resting splenocytes of $Klf13^{+/+}$ mice, KLF13 is expressed at low levels but increases after activation (Fig. 1*D*, lanes 1 and 3). In $Klf13^{-/-}$ mice, no *Klf13* mRNA was detectable by PCR (data not shown) and no KLF13 protein was identified by Western blot in either thymocytes (Fig. 1*C*, lanes 2 and 4) or splenocytes (Fig. 1*D*, lanes 2 and 4). T lymphocytes isolated from spleens of $Klf13^{-/-}$ mice expressed less RANTES 5 days after activation than did cells from $Klf13^{+/+}$ mice (Fig. 1*E*).

Enlarged lymphoid organs in *Klf13*$^{-/-}$ mice

Klf13$^{-/-}$ mice were grossly normal but, upon pathological examination, were found to have enlarged thymi and spleens, as well as increased total thymocytes and splenocytes (Fig. 2, *A* and *B*), suggesting a defect not directly related to RANTES expression. Increased numbers of thymocytes in *Klf13*$^{-/-}$ mice compared with *Klf13*$^{+/+}$ littermates was most pronounced in young mice and decreased over time (Fig. 2*C*), whereas the total number of splenocytes was increased in *Klf13*$^{-/-}$ mice at all ages examined compared with *Klf13*$^{+/+}$ littermates (Fig. 2*D*). In comparison to wild-type mice, the percentage of CD4^{+}CD8^{+} cells in the thymus were consistently increased in *Klf13*$^{-/-}$ mice (Table I), indicating that these cells contribute to the increased number of total thymocytes. In addition, TCRβ^{+} thymocytes were decreased in *Klf13*$^{-/-}$ mice, whereas no significant differences of the percentages of other lymphocyte subsets from blood, peritoneum, or spleen were observed (Table I). Pathological examination showed normal organization of thymus and spleen in *Klf13*$^{-/-}$ mice, suggesting that the enlargement of both spleen and thymus is not due to lymphocyte infiltration from nonlymphoid organs (data not shown). Although KLF13 activates the promoters for γ-globin and SM22α and represses the promoter for cytochrome P450 CYP1A1 in vitro (11–14), no gross defects in hemopoietic or smooth muscle cells were detected in *Klf13*$^{-/-}$ mice.

Lymphoid cells from *Klf13*$^{+/+}$ and *Klf13*$^{-/-}$ mice exhibit similar patterns of cell proliferation, whereas thymocytes from Klf13$^{-/-}$ mice are more resistant to apoptosis

Potential mechanisms contributing to the enlarged lymphoid organs in *Klf13*$^{-/-}$ mice include increased cell proliferation or decreased cell death. To differentiate between these possibilities, proliferation and survival were evaluated in cells from bone marrow and thymus from *Klf13*$^{+/+}$ and *Klf13*$^{-/-}$ mice. No differences in cell proliferation, as measured by BrdU uptake, were detected in these cells (Fig. 3*A*). Cell division of CFSE-labeled CD4^{+} and CD8^{+} splenocytes was similar in *Klf13*$^{+/+}$ and *Klf13*$^{-/-}$ mice (Fig. 3*B*). Several approaches were taken to investigate whether reduced apoptosis contributed to thymic enlargement. TUNEL assay was used to measure the spontaneous cell death rate of thymocytes without in vitro culture. The percentage of apoptotic cells in thymocytes from *Klf13*$^{-/-}$ mice was reduced compared with *Klf13*$^{+/+}$ littermates (Fig. 4*A*). In addition, thymocytes from *Klf13*$^{-/-}$ mice showed prolonged cell survival compared with cells from *Klf13*$^{+/+}$ littermates under conditions approximating spontaneous or activated cell death (Fig. 4, *B* and *C*). When cultured with staurosporine, an apoptosis-inducing agent, both thymocytes and splenocytes from *Klf13*$^{-/-}$ mice were more resistant to apoptosis than those from wild-type littermates (Fig. 4*D*). This result was also true for CD3^{+} T cells and B220^{+} B cells isolated from spleens. Thus, thymocytes and splenocytes from *Klf13*$^{-/-}$ mice are more resistant to cell death than their *Klf13*$^{+/+}$ counterparts.

KLF13 inhibits expression of BCL-X_L

Because *Klf13*$^{-/-}$ mice have enlarged lymphoid organs and a corresponding decrease in lymphoid cell apoptosis, cDNA microarrays were used to identify molecule(s) that might be involved in this unexpected phenotype and rt-qPCR was used to confirm these data. Both microarray and rt-qPCR showed that the expression of the antiapoptotic molecule, *Bcl-xL*, was elevated in *Klf13*$^{-/-}$ thymocytes compared with *Klf13*$^{+/+}$ littermates (Table II and Fig. 5*A*). We also examined other molecules involved in apoptosis, including *Bcl-2* and caspase family members as well as *Apaf1*, but did not find any other differences that were detected by both methods (Table II). Western blot analyses confirmed the observation that there was a significant increase in expression in BCL-X_L in thymocytes and splenocytes from *Klf13*$^{-/-}$ mice compared with *Klf13*$^{+/+}$ littermates (Fig. 5*B*). BCL-X_L expression in thymocytes and splenocytes from *Klf13*$^{+/-}$ mice was also examined by rt-qPCR and Western blot, and the levels were found to be intermediate between *Klf13*$^{+/+}$ mice and *Klf13*$^{-/-}$ mice (Fig. 5, *A* and

B). Although the majority of thymocytes are $CD4^+CD8^+$, it is the single-positive (SP) thymocytes that eventually emigrate to peripheral lymphoid tissues, including the spleen where they reside as mature T cells. Therefore, we sorted $CD4^+CD8^-$ thymocytes and examined *Bcl-xL* expression. Due to the limited number of sorted $CD4^+CD8^-$ cells obtained from each thymus, we were only able to assay *Bcl-xL* expression by rt-qPCR and not by Western blot. The even smaller population of $CD4^-CD8^+$ thymocytes did not allow examination of this cell type for BCL-X_L expression by either method. For $CD4^+CD8^-$ thymocytes, there was a significant increase in *Bcl-xL* expression in $Klf13^{-/-}$ mice compared with their $Klf13^{+/+}$ littermates (Fig. 5*C*), suggesting that mature T cells in the periphery may be more resistant to apoptosis. This observation is consistent with the fact that $CD3^+$ splenic T cells from $Klf13^{-/-}$ mice are more resistant to apoptosis than those from $Klf13^{+/+}$ littermates (Fig. 4*D*). In addition, the fold increase in *Bcl-xL* mRNA observed in $CD4^+CD8^-$ cells was much greater than that seen in total thymocytes, which may be due to a masking effect by the total cell population.

The murine *Bcl-xL* promoter contains a number of potential KLF13 binding sites (Fig. 6*A* and Ref. 16). EMSA demonstrates that KLF13 can bind to multiple sites of the *Bcl-xL* promoter (Fig. 6*B*). To assess the effect of KLF13 on mouse *Bcl-xL* expression and to determine whether these multiple KLF13 binding sites are functional, a series nested deletions and sequential 300-bp regions from ~−1,800 to −1 bp relative to the translational start site were cloned into a luciferase reporter construct (Fig. 6*C*). These constructs were cotransfected with KLF13 into NIH 3T3 cells. KLF13 caused a significant decrease in reporter gene activity of the *Bcl-xL* promoter from each of the deletion constructs tested, suggesting that at least one putative binding site in each 300-bp region is functional. In addition, the greatest basal activity of the *Bcl-xL* promoter was found in the region from −1,800 to −1,500 bp, and deletion of this region caused a significant decrease in overall activity.

Discussion

We demonstrate here that disruption of the *Klf13* gene results in mice with enlarged lymphoid organs. This phenotype is associated with decreased apoptosis and increased expression of BCL-X_L. Activated T lymphocytes from $Klf13^{-/-}$ mice produce less RANTES than cells from $Klf13^{+/+}$ littermates. Thus, KLF13 is a positive regulator of RANTES and a negative regulator of BCL-X_L in vivo.

Previous experiments suggest a dual role for KLF13, as well as family members KLF9 (BTEB-1), KLF1 (EKLF), KLF4 (GKLF), and KLF2 (LKLF), as both activators and repressors in vitro (1,7,11–13,17). Leiden and colleagues (18,19) generated $Klf2^{-/-}$, $Rag2^{-/-}$ mice with peripheral T lymphocyte defects, including decreased numbers of peripheral T lymphocytes and abnormal cell surface phenotypes ($CD44^{high}$, $CD69^{high}$, L $selectin^{low}$), suggesting that peripheral T lymphocytes were spontaneously activated. They showed that $Klf2^{-/-}$ lymphocytes expressed increased Fas ligand and suggested that they were deleted by this mechanism. Thus, the $Klf2^{-/-}$ phenotype, in many ways the opposite of the phenotype observed in $Klf13^{-/-}$ mice, does not involve BCL-2 family members.

Results from in vitro studies suggest possible mechanisms by which KLF13 can repress and activate transcription. Some KLFs (KLF3 (BKLF), KLF8 (BKLF3), and KLF12 (AP-2rep)) repress transcription by binding to the cellular protein CtBP (C-terminal binding protein) (20–22); other KLFs suppress transcription by interacting with corepressors mSin3a and histone deacetylase (23–26); whereas KLF2 binds an E3 ubiquitin ligase (27). In all of these cases, transcriptional repression is mediated by interaction with corepressors. Kaczynski et al. (13,14) identified three repression domains in the KLF13 amino terminus that interact with the mSin3A histone deacetylase corepressor complex, repressing CYP1A1. Thus, KLF13 may

decrease expression of *Bcl-xL* through corepressors that deacetylate histones, changing histone structure and blocking transcription. In contrast, transcriptional activation by KLF13 is associated with acetylation, the likely process regulating *RANTES* expression. Song et al. (28) demonstrated that the histone acetyltransferases, p300/cyclic AMP response element binding protein (CBP) and p300/CBP-associated factor (PCAF), interact in regulation of KLF13. Contingent upon the cellular context and kinetics of binding, these factors result in assembly or disassembly of the complex depending upon the acetylation state. We recently reported that KLF13 serves as a lynchpin for recruitment of a large molecular complex to the RANTES promoter that includes the MAPK Nemo-like kinase, p300/CBP, PCAF, and the ATPase BRG-1 (Brahma-related gene 1) (29). This “enhancesome” regulates gene expression via acetylation and phosphorylation. The ensuing effects of this dynamic complex on chromatin structure, at least in part, explain the ability of KLF13 to function as either a repressor or activator of gene expression.

Others have published widely on the role of BCL-X_L as an inhibitor of apoptosis both in vitro and in vivo (30,31). Lymphocytes from transgenic mice overexpressing BCL-X_L exhibit increased cell survival and resistance to apoptotic stimuli (30,31), analogous to the phenotype we describe here. However, in contrast to studies in *Bcl-xL* transgenic mice, we see minimal effects on cell phenotype or on positive or negative selection. There is no evidence for tumorigenesis or autoimmunity in *Klf13*$^{-/-}$ mice. Thus, overexpression of BCL-X_L in transgenic mice is functionally different from the increased levels of these proteins induced by *Klf13* deletion.

BCL-X_L expression is regulated by various proteins including the STAT and Rel/NF-κB transcription factor families that play distinct roles in many different cell types (32). Mice that lack STAT3 in T cells have decreased IL-6-induced proliferation due to impairment of IL-6-mediated survival (33). Fetal liver cells derived from p50/p60 double-knockout mice are blocked in development at an early stage and are unable to generate B and T cells, suggesting an essential role of NF-κB in lymphocyte development (34). However, in our system, the levels of mRNA expression of STAT family members (STAT-1, -3, and -5) and NF-κB did not change in *Klf13*$^{-/-}$ thymocytes and splenocytes, although BCL-X_L expression was increased in these cells compared with those of their *Klf13*$^{+/+}$ littermates (data not shown). This result suggests that additional factors contribute to the regulation of BCL-X_L expression in lymphocytes. KLF13 appears to be one of these factors and serves as a negative regulator of BCL-X_L in thymocytes and splenocytes.

The potential functional consequences of KLF13 increasing RANTES expression and decreasing BCL-X_L expression are as follows: 1) chemokine attraction of a robust inflammatory infiltrate composed of lymphocytes, monocytes, and eosinophils, and 2) increased susceptibility of the chemokine-producing cells to apoptotic signals. Thus, KLF13 contributes to inflammation by recruiting an immune infiltrate but then turns off this response via apoptosis.

References

1. Kaczynski J, Cook T, Urrutia R. Sp1- and Kruppel-like transcription factors. Genome Biol 2003;4:206. [PubMed: 12620113]
2. Song A, Chen YF, Thamatrakoln K, Storm TA, Krensky AM. RFLAT-1: a new zinc finger transcription factor that activates RANTES gene expression in T lymphocytes. Immunity 1999;10:93–103. [PubMed: 10023774]
3. Nelson PJ, Pattison JM, Krensky AM. Gene expression of RANTES. Methods Enzymol 1997;287:148–162. [PubMed: 9330320]

4. Schall TJ, Jongstra J, Dyer BJ, Jorgensen J, Clayberger C, Davis MM, Krensky AM. A human T cell-specific molecule is a member of a new gene family. J. Immunol 1988;141:1018–1025. [PubMed: 2456327]
5. Miyamoto NG, Medberry PS, Hesselgesser J, Boehlk S, Nelson PJ, Krensky AM, Perez HD. Interleukin-1β induction of the chemokine RANTES promoter in the human astrocytoma line CH235 requires both constitutive and inducible transcription factors. J. Neuroimmunol 2000;105:78–90. [PubMed: 10713367]
6. Nelson PJ, Ortiz BD, Pattison JM, Krensky AM. Identification of a novel regulatory region critical for expression of the RANTES chemokine in activated T lymphocytes. J. Immunol 1996;157:1139–1148. [PubMed: 8757619]
7. Song A, Nikolcheva T, Krensky AM. Transcriptional regulation of RANTES expression in T lymphocytes. Immunol. Rev 2000;177:236–245. [PubMed: 11138780]
8. Scohy S, Gabant P, Van Reeth T, Hertveldt V, Dreze PL, Van Vooren P, Riviere M, Szpirer J, Szpirer C. Identification of KLF13 and KLF14 (SP6), novel members of the SP/XKLF transcription factor family. Genomics 2000;70:93–101. [PubMed: 11087666]
9. Rekdal C, Sjottem E, Johansen T. The nuclear factor SPBP contains different functional domains and stimulates the activity of various transcriptional activators. J. Biol. Chem 2000;275:40288–40300. [PubMed: 10995766]
10. Nikolcheva T, Pyronnet S, Chou SY, Sonenberg N, Song A, Clayberger C, Krensky AM. A translational rheostat for RFLAT-1 regulates RANTES expression in T lymphocytes. J. Clin. Invest 2002;110:119–126. [PubMed: 12093895]
11. Asano H, Li XS, Stamatoyannopoulos G. FKLF-2: a novel Kruppel-like transcriptional factor that activates globin and other erythroid lineage genes. Blood 2000;95:3578–3584. [PubMed: 10828046]
12. Martin KM, Cooper WN, Metcalfe JC, Kemp PR. Mouse BTEB3, a new member of the basic transcription element binding protein (BTEB) family, activates expression from GC-rich minimal promoter regions. Biochem. J 2000;345:529–533. [PubMed: 10642511]
13. Kaczynski JA, Conley AA, Fernandez Zapico M, Delgado SM, Zhang JS, Urrutia R. Functional analysis of basic transcription element (BTE)-binding protein (BTEB) 3 and BTEB4, a novel Sp1-like protein, reveals a subfamily of transcriptional repressors for the BTE site of the *cytochrome P4501A1* gene promoter. Biochem. J 2002;366:873–882. [PubMed: 12036432]
14. Kaczynski J, Zhang JS, Ellenrieder V, Conley A, Duenes T, Kester H, van Der Burg B, Urrutia R. The Sp1-like protein BTEB3 inhibits transcription via the basic transcription element box by interacting with mSin3A and HDAC-1 co-repressors and competing with Sp1. J. Biol. Chem 2001;276:36749–36756. [PubMed: 11477107]
15. Dong C, Li Q, Lyu SC, Krensky AM, Clayberger C. A novel apoptosis pathway activated by the carboxyl terminus of p21. Blood 2005;105:1187–1194. [PubMed: 15466931]
16. Grillot DA, Gonzalez-Garcia M, Ekhterae D, Duan L, Inohara N, Ohta S, Seldin MF, Nunez G. Genomic organization, promoter region analysis, and chromosome localization of the mouse bcl-x gene. J. Immunol 1997;158:4750–4757. [PubMed: 9144489]
17. Song A, Patel A, Thamatrakoln K, Liu C, Feng D, Clayberger C, Krensky AM. Functional domains and DNA-binding sequences of RFLAT-1/KLF13, a Kruppel-like transcription factor of activated T lymphocytes. J. Biol. Chem 2002;277:30055–30065. [PubMed: 12050170]
18. Kuo CT, Veselits ML, Barton KP, Lu MM, Clendenin C, Leiden JM. The LKLF transcription factor is required for normal tunica media formation and blood vessel stabilization during murine embryogenesis. Genes Dev 1997;11:2996–3006. [PubMed: 9367982]
19. Kuo CT, Veselits ML, Leiden JM. LKLF: A transcriptional regulator of single-positive T cell quiescence and survival. Science 1997;277:1986–1990. [PubMed: 9302292]
20. Schuierer M, Hilger-Eversheim K, Dobner T, Bosserhoff AK, Moser M, Turner J, Crossley M, Buettner R. Induction of AP-2α expression by adenoviral infection involves inactivation of the AP-2rep transcriptional corepressor CtBP1. J. Biol. Chem 2001;276:27944–27949. [PubMed: 11373277]
21. van Vliet J, Turner J, Crossley M. Human Kruppel-like factor 8: a CACCC-box binding protein that associates with CtBP and represses transcription. Nucleic Acids Res 2000;28:1955–1962. [PubMed: 10756197]

22. Turner J, Crossley M. Cloning and characterization of mCtBP2, a co-repressor that associates with basic Kruppel-like factor and other mammalian transcriptional regulators. EMBO J 1998;17:5129–5140. [PubMed: 9724649]

23. Chen X, Bieker JJ. Unanticipated repression function linked to erythroid Kruppel-like factor. Mol. Cell. Biol 2001;21:3118–3125. [PubMed: 11287616]

24. Ellenrieder V, Zhang JS, Kaczynski J, Urrutia R. Signaling disrupts mSin3A binding to the Mad1-like Sin3-interacting domain of TIEG2, an Sp1-like repressor. EMBO J 2002;21:2451–2460. [PubMed: 12006497]

25. Fleischer TC, Yun UJ, Ayer DE. Identification and characterization of three new components of the mSin3A corepressor complex. Mol. Cell. Biol 2003;23:3456–3467. [PubMed: 12724404]

26. Zhang JS, Moncrieffe MC, Kaczynski J, Ellenrieder V, Prendergast FG, Urrutia R. A conserved α-helical motif mediates the interaction of Sp1-like transcriptional repressors with the corepressor mSin3A. Mol. Cell. Biol 2001;21:5041–5049. [PubMed: 11438660]

27. Conkright MD, Wani MA, Lingrel JB. Lung Kruppel-like factor contains an autoinhibitory domain that regulates its transcriptional activation by binding WWP1, an E3 ubiquitin ligase. J. Biol. Chem 2001;276:29299–29306. [PubMed: 11375995]

28. Song CZ, Keller K, Murata K, Asano H, Stamatoyannopoulos G. Functional interaction between coactivators CBP/p300, PCAF, and transcription factor FKLF2. J. Biol. Chem 2002;277:7029–7036. [PubMed: 11748222]

29. Ahn YT, Huang B, McPherson L, Clayberger C, Krensky AM. Dynamic interplay of transcriptional machinery and chromatin regulates “late” expression of the chemokine RANTES in T lymphocytes. Mol. Cell. Biol 2007;27:253–266. [PubMed: 17074812]

30. Chao DT, Korsmeyer SJ. BCL-2 family: regulators of cell death. Annu. Rev. Immunol 1998;16:395–419. [PubMed: 9597135]

31. Chao DT, Korsmeyer SJ. BCL-XL-regulated apoptosis in T cell development. Int. Immunol 1997;9:1375–1384. [PubMed: 9310841]

32. Grad JM, Zeng XR, Boise LH. Regulation of Bcl-xL: a little bit of this and a little bit of STAT. Curr. Opin. Oncol 2000;12:543–549. [PubMed: 11085453]

33. Takeda K, Kaisho T, Yoshida N, Takeda J, Kishimoto T, Akira S. Stat3 activation is responsible for IL-6-dependent T cell proliferation through preventing apoptosis: generation and characterization of T cell-specific Stat3-deficient mice. J. Immunol 1998;161:4652–4660. [PubMed: 9794394]

34. Horwitz BH, Scott ML, Cherry SR, Bronson RT, Baltimore D. Failure of lymphopoiesis after adoptive transfer of NF-κB-deficient fetal liver cells. Immunity 1997;6:765–772. [PubMed: 9208848]

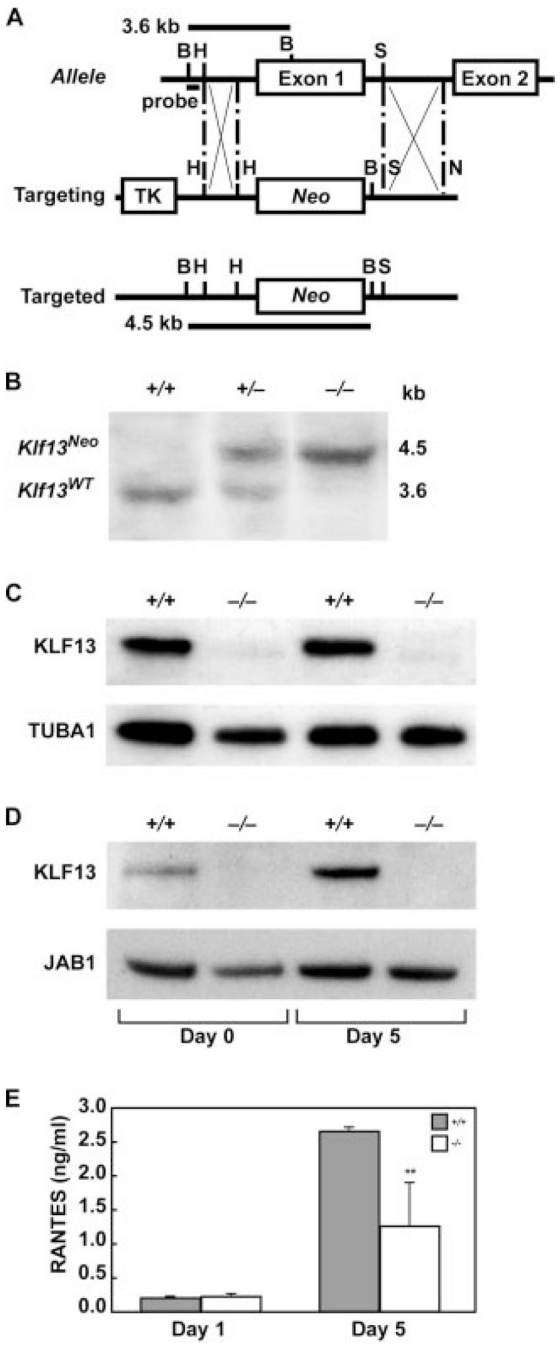

FIGURE 1.

Targeted disruption of the *Klf13* gene. *A*, Schematic representation of the wild-type *Klf13* allele, the targeting vector, and the predicted targeted allele are shown. In the targeted *Klf13* allele, *Neo* replaces exon 1 plus 0.7 kb upstream and 0.6 kb downstream of the *Klf13* gene. B, *Bam*HI; H, *Hin*dIII; S, *Sac*II; N, *Not*I; TK, thymidine kinase; *Neo*, neomycin resistance. *B*, Southern blot analysis of genomic DNA from wild-type (+/+), heterozygous (+/−), and homozygous (−/−) mice. After *Bam*HI digestion, the wild-type allele ($Klf13^{WT}$) is detected as a 3.6-kb fragment, whereas the targeted allele ($Klf13^{Neo}$) is detected as a 4.5-kb fragment using probe as indicated in Fig. 1*A*. *C*, Western blot of KLF13 expression in thymocytes from two littermate pairs of wild-type (+/+) and mutant (−/−) mice, with TUBA1 used as an internal

control. *D*, Western blot of KLF13 expression in splenocytes, with JAB1 used as an internal control. Splenocytes from *Klf13*$^{+/+}$ and *Klf13*$^{-/-}$ littermates were left untreated (Day 0) or activated with anti-CD3 and anti-CD28 Abs for 5 days (Day 5). *E*, KLF13 positively regulates RANTES expression in T lymphocytes. Splenic CD3^{+} T lymphocytes isolated from *Klf13*$^{+/+}$ and *Klf13*$^{-/-}$ littermates were stimulated with anti-CD3 and anti-CD28 Abs. Supernatants were removed on day 1 and day 5 and RANTES was measured by ELISA. Data presented are the mean ± SD from three pairs of littermates (**, $p < 0.01$).

A

	+/+	+/-	-/-
Thymus (mg)	58 ± 7.9	62 ± 8.6	80 ± 10*
Spleen (mg)	89 ± 5.2	99.7 ± 17.6	127.3 ± 8.1***
Thymocytes (x 10^6)	144.7 ± 5.0	178.7 ± 16.8*	203 ± 16.8***
Splenocytes (x 10^6)	138.7 ± 15.2	161.7 ± 24.1	197 ± 13.5***

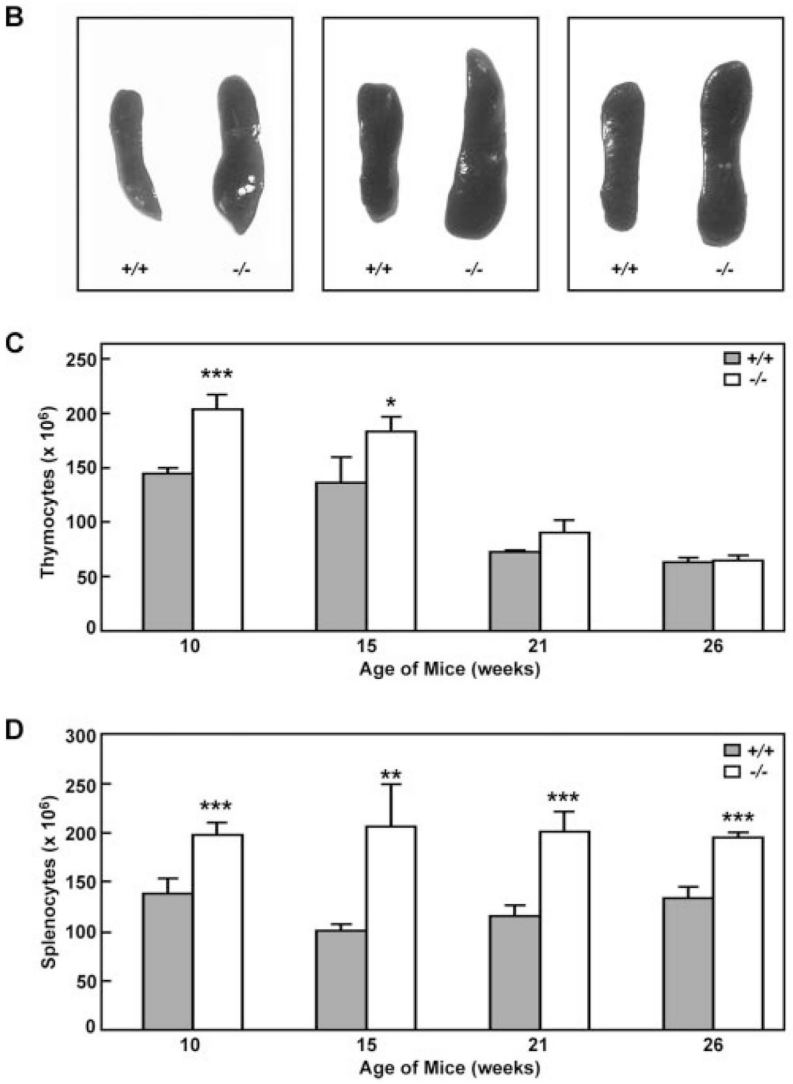

FIGURE 2.

Phenotypic comparison of thymus and spleen from *Klf13*$^{+/+}$, *Klf13*$^{+/-}$, and *Klf13*$^{+/-}$ littermates. *A*, Increased mass of lymphoid organs and increased numbers of thymocytes and splenocytes in *Klf13*$^{-/-}$ mice. Three sets of littermates were subjected to pathological examination and all other parameters examined were normal. *B*, Enlarged spleens of *Klf13*$^{-/-}$ mice from three pairs of littermates. *C*, Increased numbers of thymocytes in *Klf13*$^{-/-}$ mice at different ages as indicated. All values are the mean ± SD from three pairs of littermates (*, $p < 0.05$ and ***, $p < 0.001$). *D*, Increased numbers of splenocytes in *Klf13*$^{-/-}$ mice at different ages as indicated. All values are the mean ± SD from three pairs of littermates (**, $p < 0.01$ and ***, $p < 0.001$).

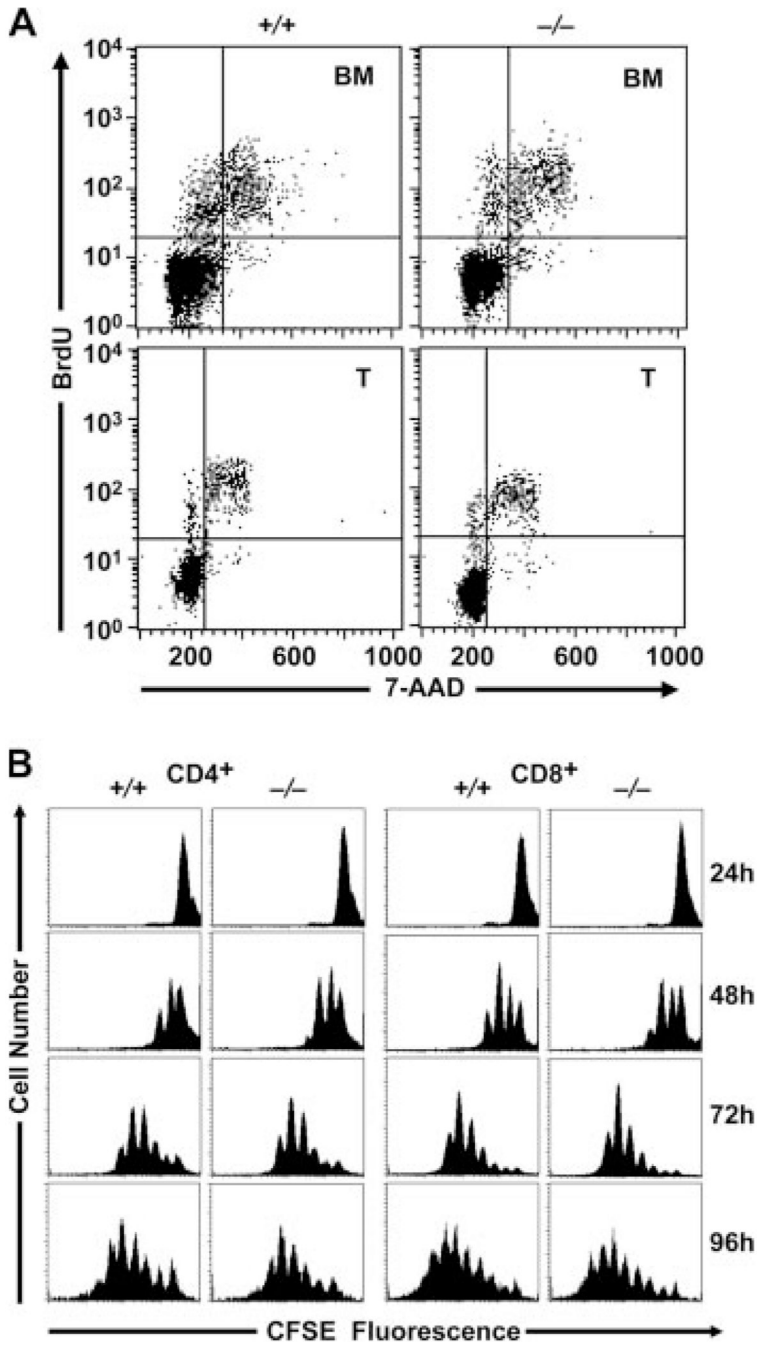

FIGURE 3.

Normal proliferation and cell division in cells from *Klf13*$^{-/-}$ mice. *A*, Incorporation of BrdU into bone marrow cells (BM, *top panels*) and thymocytes (T, *bottom panels*) from *Klf13*$^{+/+}$ and *Klf13*$^{-/-}$ mice. *B*, Cell division in activated *Klf13*$^{+/+}$ and *Klf13*$^{-/-}$ CD4^{+} or CD8^{+} splenocytes. CFSE-labeled cells were cultured in vitro with anti-CD3 and anti-CD28 Abs and analyzed by flow cytometry at the indicated times. For both experiments, three littermate pairs were tested and data from one littermate pair are presented.

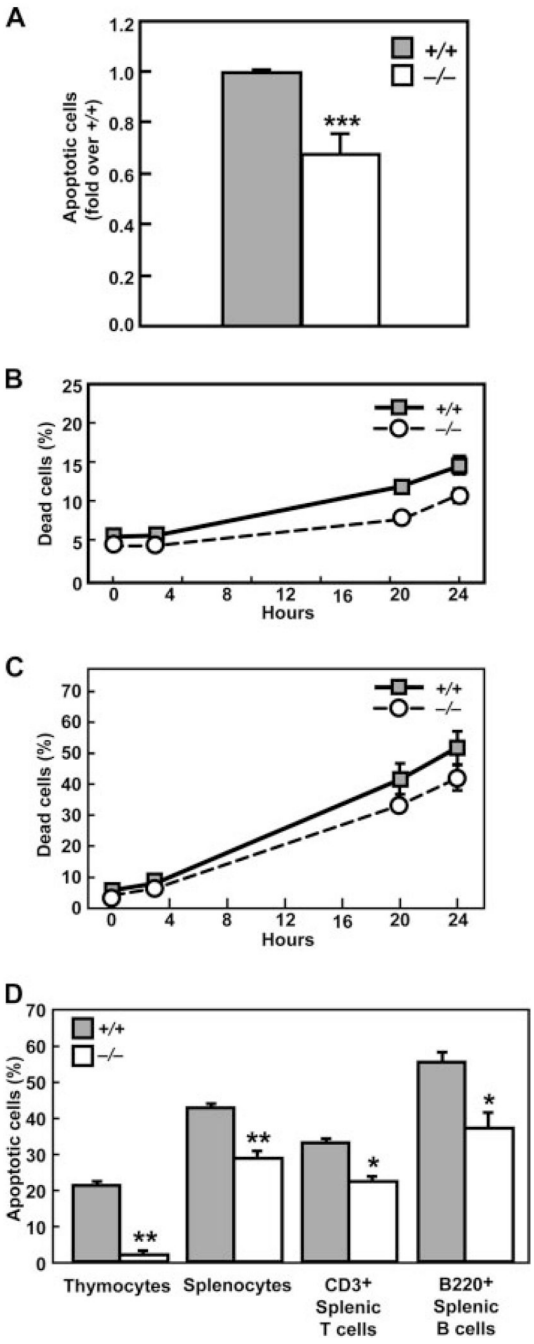

FIGURE 4.

Thymocytes in *Klf13*$^{-/-}$ mice exhibit defective cell death. *A*, TUNEL assay. Fold decrease in apoptotic cells of thymocytes in *Klf13*$^{-/-}$ mice in comparison to *Klf13*$^{+/+}$ mice. Data are the mean ± SD from three pairs of littermates (***, $p < 0.001$). *B*, *Klf13*$^{-/-}$ thymocytes are more resistant to spontaneous cell death when cultured in vitro. Data are the mean ± SD from three pairs of littermates. Differences between *Klf13*$^{+/+}$ and *Klf13*$^{-/-}$ mice were analyzed by ANOVA and shown to be significant ($p < 0.0001$). *C*, *Klf13*$^{-/-}$ thymocytes are more resistant to activation-induced cell death than *Klf13*$^{+/+}$ thymocytes when cultured in vitro with Con A (10 μg/ml). Data are the mean ± SD from three pairs of littermates. Differences between *Klf13*$^{+/+}$ and *Klf13*$^{-/-}$ mice were analyzed by ANOVA and shown to be significant ($p <$

0.0017). *D*, Cells from *Klf13*$^{-/-}$ mice are more resistant to staurosporine-induced apoptosis compared with *Klf13*$^{+/+}$ mice. Three littermate pairs were tested in triplicate and data from one littermate pair are presented as the mean ± SD (**, $p < 0.01$ and ***, $p < 0.001$).

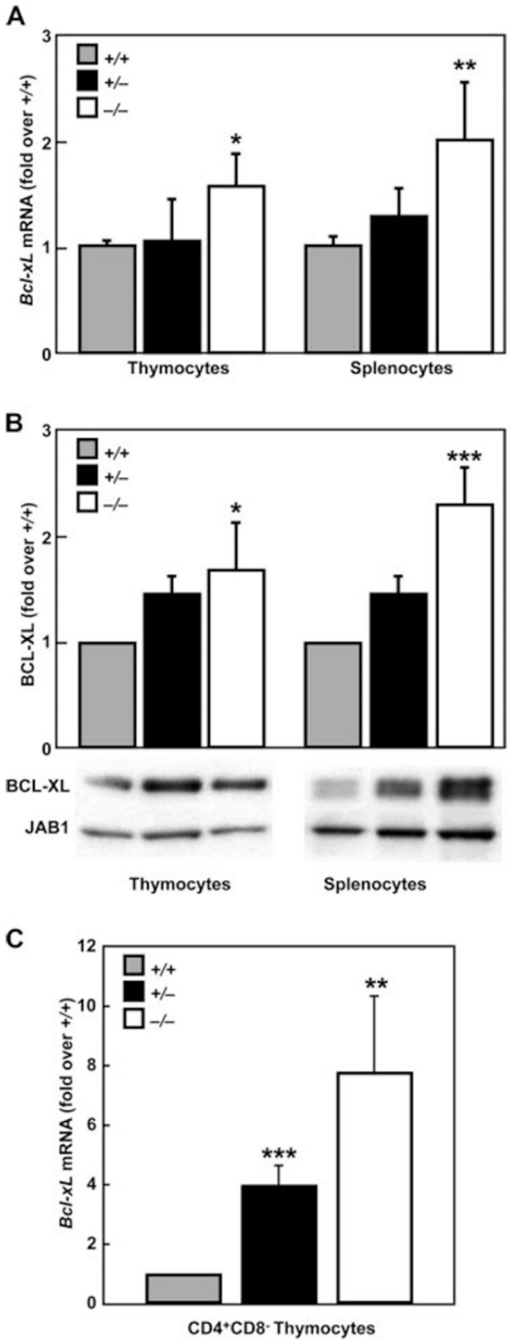

FIGURE 5.

Increased expression of BCL-X_L in thymocytes and splenocytes from *Klf13*$^{-/-}$ mice. *A*, rt-qPCR analysis. Fold increase in *Bcl-xL* expression in thymocytes and splenocytes of *Klf13*$^{-/-}$ and *Klf13*$^{+/-}$ mice compared with *Klf13*$^{+/+}$ mice was measured by rt-qPCR and normalized by *Gusb*. Values are the mean ± SD for three sets of littermates (*, $p < 0.05$ and **, $p < 0.01$). *B*, Western blot analysis. Fold increase in BCL-X_L expression in thymocytes and splenocytes of *Klf13*$^{-/-}$ and *Klf13*$^{+/-}$ mice compared with *Klf13*$^{+/+}$ mice was detected in whole cell lysates and normalized to JAB1. Quantitation was performed by densitometry and values are graphed as the mean ± SD from three sets of littermates (*, $p < 0.05$ and ***, $p < 0.001$). Blots shown are representative of one littermate set. *C*, rt-qPCR analysis of

$CD4^+CD8^-$ thymocytes. Fold increase in *Bcl-xL* expression in $CD4^+CD8^-$ cells of $Klf13^{-/-}$ and $Klf13^{+/-}$ mice compared with $Klf13^{+/+}$ mice was measured by rt-qPCR and normalized by *Gusb*. Values are the mean ± SD for three sets of littermates (*, $p < 0.05$ and **, $p < 0.01$).

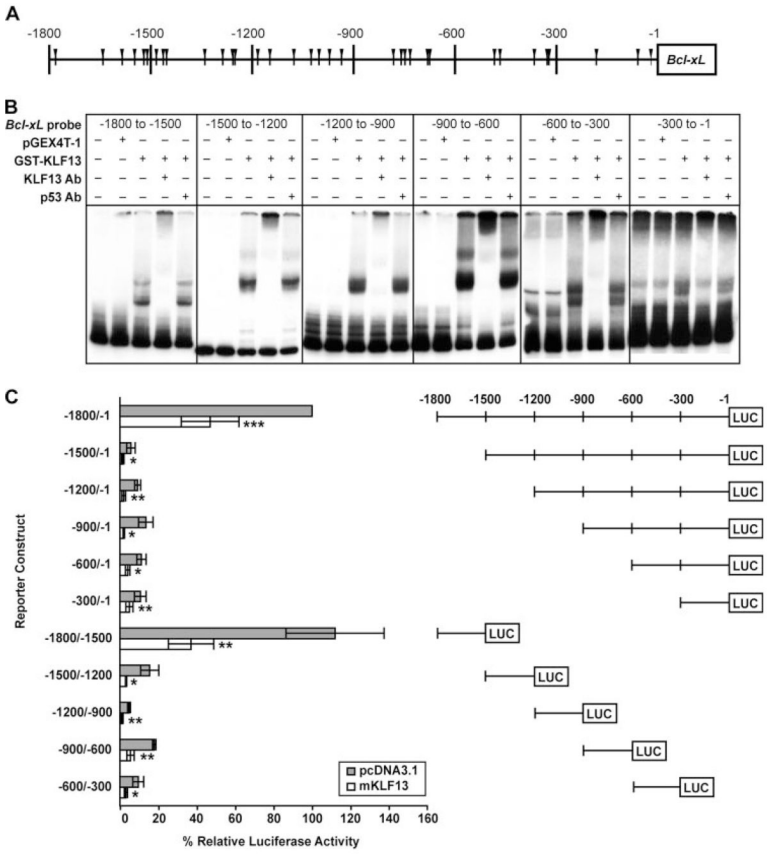

FIGURE 6.

KLF13 is a negative regulator of *Bcl-xL* expression. *A*, Schematic representation of the *Bcl-xL* promoter showing KLF13 consensus binding sites (**|**). Numbers are relative to the +1 *Bcl-xL* translational start site. *B*, EMSA of recombinant GST-KLF13 binding to the *Bcl-xL* promoter was performed using probes corresponding to sequential 300-bp regions of the *Bcl-xL* promoter from −1,800 to −1 bp relative to the translational start site. Purified GST from empty pGEX4T-1 vector was used as a negative control. Supershift using anti-KLF13 Ab or a negative control Ab (p53 Ab) is indicated. *C*, KLF13 represses *Bcl-xL* promoter activity. NIH3T3 cells were cotransfected with a series of luciferase reporter constructs containing nested deletions or sequential 300-bp regions of the *Bcl-xL* promoter from −1,800 to −1 bp relative to the translational start site as indicated, and either pcDNA3.1(+) or mouse KLF13 expression plasmid. Luciferase activity was measured in cell lysates from transfected cells and normalized by total cellular protein concentration. Values are the mean ± SD for three independent transfections (*, $p < 0.05$, **, $p < 0.01$, and ***, $p < 0.001$).

Table I

FACS analysis of lymphocyte subsets in *Klf13*$^{+/+}$ and *Klf13*$^{-/-}$ mice[a]

		% of Cells	
	Subsets	***Klf13***$^{+/+}$	***Klf13***$^{-/-}$
Thymus	SP (CD4$^+$)	8.01 ± 1.3	5.9 ± 1.4
	SP (CD8$^+$)	2.3 ± 0.8	1.5 ± 0.2
	DP (CD4$^+$ CD8$^+$)	86.6 ± 1.3	89.9 ± 1.4*
	DN (CD4$^-$CD8$^-$)	2.5 ± 1.4	1.9 ± 0.9
	TCRβ	38.28 ± 3.7	25.84 ± 4.29*
Blood	T cells (CD3$^+$)	30.9 ± 2.7	29.0 ± 0.55
	B cells (B220$^+$)	23.7 ± 10.1	22.2 ± 7.9
	NK cells (NK1.1$^+$)	7.5 ± 2.6	5.1 ± 1.0
Peritoneum	T cells (CD3$^+$)	18.5 ± 6.3	12.7 ± 2.3
	B cells (B220$^+$)	31.0 ± 12.0	35.7 ± 7.6
	NK cells (NK1.1$^+$)	0.8 ± 0.2	1.2 ± 0.4
Spleen	T cells (CD3$^+$)	38.3 ± 4.9	31.4 ± 11.0
	(CD3$^+$CD4$^+$)	23.7 ± 4.5	17.3 ± 3.8
	(CD3$^+$CD8$^+$)	14.7 ± 0.4	14.2 ± 7.5
	B cells (B220$^+$)	39.2 ± 10.2	36.4 ± 11.0
	NK cells (NK1.1$^+$)	9.5 ± 3.9	6.9 ± 2.7
	TCRβ	34.7 ± 10.0	30.4 ± 8.5
	TCRγδ	1.1 ± 0.4	1.4 ± 0.4

[a]Three pairs of mice were examined at 11–12 wk of age. Values are the mean ± SD. DP, Double positive; DN, double negative.

*$p < 0.05$.

Table II

Analysis of gene expression in thymocytes from *Klf13*$^{+/+}$ and *Klf13*$^{-/-}$ mice[a]

		Microarray	rt-qPCR
Gene Symbol	**GenBank Accession Number**	**Fold change over *Klf13*$^{+/+}$**	**Fold change over *Klf13*$^{+/+}$**
Apaf1	NM_009684	0.52 ± 0.05***	1.16 ± 0.25
Bad	NM_007522	1.36 ± 0.31	1.13 ± 0.13
Bag-1	NM_009736	1.03 ± 0.53	1.15 ± 0.34
Bag-3	NM_013863	0.50 ± 0.12***	1.15 ± 0.14
Bag-4	NM_026121	0.45 ± 0.05**	1.28 ± 0.30
Bak1	NM_007523	1.98 ± 0.23	0.93 ± 0.25
Bax	NM_007527	1.41 ± 0.60	1.2 ± 0.02***
Bbc3	NM_133234	0.58 ± 0.17**	1.49 ± 0.54
Bcl2	NM_177410	1.54 ± 0.75	1.22 ± 0.25
Bcl-X$_L$	NM_009743	2.38 ± 0.35***	1.61 ± 0.31**
Bcl2l2	NM_007537	1.29 ± 0.70	1.32 ± 0.27**
Bcl2l10	NM_013479	N/A	N/A
Bcl2l11	NM_207680	0.57 ± 0.08	1.05 ± 0.29
Bid	NM_007544	N/A	1.55 ± 0.37**
Bid3	NM_007545	0.39 ± 0.13***	N/A
Bik	NM_007546	N/A	1.06 ± 0.19
Bnip2	NM_016787	N/A	0.92 ± 0.26
Bnip3	NM_009760	N/A	1.12 ± 0.42
Bnip3L	NM_009761	2.2 ± 0.27	1.09 ± 0.24
Bok	NM_016778	1.90 ± 0.70	0.99 ± 0.34
Mcl1	NM_008562	2.44 ± 0.29	0.82 ± 0.14**
Casp1	NM_009807	0.46 ± 0.12***	1.17 ± 0.84
Casp2	NM_007610	2.16 ± 0.20***	1.01 ± 0.28
Casp3	NM_009810	2.33 ± 0.21***	1.36 ± 0.37
Casp4	NM_007609	N/A	0.82 ± 0.27
Casp6	NM_009811	1.98 ± 0.49	0.76 ± 0.19**
Casp7	NM_007611	1.20 ± 0.17	1.62 ± 0.59
Casp8	NM_009812	1.28 ± 0.72	0.81 ± 0.18
Casp9	NM_015733	1.31 ± 0.46	0.96 ± 0.26
Casp12	NM_009808	N/A	1.21 ± 0.56
Casp14	NM_009809	0.59 + 0.04	N/A

[a] Three pairs of mice were examined at 11–12 wk of age. Values are the mean ± SD.

** $p < 0.01$

*** $p < 0.001$.